Article

Discovery Medicine 2025; 37(201): 2411–2427
https://doi.org/10.24976/Discov.Med.202537201.204

Histone Lactylation Promotes Transcriptional Activation of YTHDF2 in High Glucose-Induced Renal Injury by Enhancing m6A Modification of GDF15

Rucui Yu[1,*], Xingxing Wang[2], Tingting Chen[1], Jingwei Xu[3]

[1]Department of Traditional Chinese Medicine, The First Affiliated Hospital of USTC, Division of Life Sciences and Medicine, University of Science and Technology of China, 230001 Hefei, Anhui, China
[2]Major of Clinical Integration of Chinese and Western Medicine, The First Clinical Medical School of Anhui University of Chinese Medicine, 230012 Hefei, Anhui, China
[3]Department of Clinical Laboratory, The First Affiliated Hospital of USTC, 230001 Hefei, Anhui, China
*Correspondence: yurucui4042301@163.com (Rucui Yu)
Submitted: 23 June 2025 Revised: 14 August 2025 Accepted: 12 September 2025 Published: 20 October 2025

Background: Diabetic nephropathy (DN) is a leading cause of end-stage renal disease, and its progression is closely associated with metabolic stress and epigenetic dysregulation under high-glucose conditions. Emerging evidence suggests that histone lactylation may play a pivotal role in gene transcription regulation during renal injury. This study aimed to elucidate the underlying mechanism by which histone lactylation of YTHDF2 exacerbates renal injury in a high-glucose environment, specifically through the enhancement of N6-methyladenosine (m6A) modification of growth differentiation factor 15 (GDF15), using both *in vivo* and *in vitro* models.

Methods: Histone lactylation and its role in renal injury were investigated in mouse renal tissues and in HK-2 tubular epithelial cells exposed to high glucose. Experimental approaches included immunofluorescence, ELISA, and immunoblotting. Autophagy and pyroptosis pathways were analyzed using markers such as LC3 and NLRP3. The histone lactylation on YTHDF2 transcription was evaluated using RT-qPCR, Chromatin immunoprecipitation (ChIP)-qPCR, and immunoblotting. Additionally, the impact of YTHDF2 on the m6A modification of GDF15 and its contribution to renal injury were examined using PAR-CLIP and MeRIP assays.

Results: Histone lactylation levels were significantly elevated in DN renal tissues and in HK2 cells exposed to high glucose ($p < 0.01$). Inhibition of histone lactylation alleviated high glucose-induced renal injury ($p < 0.01$). Interestingly, lactylation inhibition promoted autophagy while suppressing pyroptosis in both *in vivo* and *in vitro* DN models ($p < 0.05$). Histone acylation enhanced the transcriptional activation of YTHDF2, and YTHDF2 overexpression further aggravated renal injury ($p < 0.05$). Mechanistically, YTHDF2 facilitated the m6A modification of GDF15, leading to mRNA degradation and subsequent exacerbation of renal damage ($p < 0.05$).

Conclusion: Histone lactylation promotes the transcriptional activation of YTHDF2, which aggravates high glucose-induced renal injury by enhancing m6A-mediated degradation of GDF15 mRNA. Targeting the YTHDF2-GDF15 axis may represent a promising therapeutic strategy for DN.

Keywords: diabetic nephropathy; histone lactylation; YTHDF2; m6A modification; GDF15

Introduction

Diabetic nephropathy (DN) is a common microvascular complication of diabetes, characterized by persistent proteinuria and a progressive decline in glomerular filtration rate (GFR) [1]. DN significantly increases long-term morbidity and mortality and is one of the leading causes of end-stage renal disease (ESRD) [2]. Although the pathological mechanisms underlying DN have not been fully elucidated, hyperglycemia is widely considered the primary driving factor. High blood sugar levels activate various cellular signaling pathways in different types of renal cells, thereby promoting glomerular hyperfiltration. Recent studies have demonstrated that the development of DN is also closely associated with renal tubular injury and the subsequent decline in renal function [3]. Since DN is a multistage disease that often precedes clinical manifestations, renal tubular damage represents a viable therapeutic target, warranting further mechanistic investigation.

Autophagy, a cellular degradation and recycling process, plays a dual role in DN pathogenesis. Both excessive activation and insufficient activity can lead to podocyte damage. In patients with diabetes and macroalbuminuria, impaired podocyte autophagy has been observed, and reduced autophagy activity has been implicated in DN pro-

gression; conversely, restoration of autophagy may represent a promising therapeutic approach [4]. Therefore, further exploration of the molecular mechanisms of DN and the identification of novel therapeutic targets remain essential for the development of effective treatments.

Post-translational modifications (PTMs) of histones play a crucial role in maintaining cellular homeostasis by regulating DNA-dependent processes such as transcription, replication, and DNA repair. Dysregulation of histone PTMs can disrupt the balance between transcriptional activation and repression, thereby contributing to the onset and progression of various diseases [5]. In addition to well-characterized modifications such as acetylation, methylation, and phosphorylation, recent studies have identified a novel form of histone PTM – lactylation [6]. Abnormal glycolytic activity can lead to excessive production of lactic acid, which in turn induces histone lactylation and has been implicated in the pathogenesis of hypoxic pulmonary hypertension [7]. Histone lactylation has also been associated with the activation of inflammation [8]. However, to date, histone lactylation has not been reported in the context of diabetes or renal injury.

Notably, histone lactylation has been shown to enhance the transcriptional activity of the N6-methyladenosine (m6A) reader protein YTHDF2 [9]. In the context of nephropathy, YTHDF2 mediates the m6A methylation of *PPAR-*α, ultimately leading to the activation of NLRP3 inflammasome and NF-κB-driven renal inflammation [10]. In macrophages, upregulation of YTHDF2 promotes the release of lipopolysaccharide (LPS)-induced inflammatory cytokines [11]. Based on these findings, we hypothesized that YTHDF2 overexpression may contribute to the release of pro-inflammatory factors and the progression of renal injury in DN.

YTHDF2 is a well-characterized m6A reader that recognizes m6A consensus motifs and promotes the degradation of m6A-modified transcripts through recruitment of the CCR4-NOT deadenylase complex [12]. Bioinformatic analyses using StarBase and RMBase have previously showed that YTHDF2 is prone to m6A modification at the binding site on the *GDF15* gene. Interestingly, growth differentiation factor 15 (GDF15) has been reported to exert protective effects against diabetic nephropathy by inhibiting the AGE/RAGE-mediated inflammatory signaling pathway in C57BL/6 mice and HK-2 cells [13]. Therefore, we speculate that YTHDF2 may exacerbate renal injury by promoting m6A modification of GDF15 mRNA, thereby reducing its stability and impairing its anti-inflammatory function.

This study aimed to investigate the role of the YTHDF2-GDF15 axis in the progression of DN and to uncover the underlying molecular mechanism. Our findings demonstrate that high glucose levels induced increase in histone lactylation, which promotes the transcriptional activation of YTHDF2. Elevated YTHDF2 enhances the m6A modification of GDF15 mRNA, leading to its accelerated degradation and subsequent downregulation of GDF15 expression. This molecular cascade ultimately contributes to the exacerbation of renal tissue injury. Therefore, we propose that targeting the YTHDF2-GDF15 axis may represent a promising therapeutic strategy for the treatment of DN.

Materials and Methods

Construction of the Diabetic Nephropathy (DN) Mice Model

All animal experiments were approved by the Institutional Animal Use Committee of The First Affiliated Hospital of USTC (Approval No. 2023N(A)-0177). A total of 96 male C57BL/6J mice (6–8 weeks old, body weight: 18–22 g) were purchased from Beijing Vital River Laboratory Animal Technology Co., Ltd., and housed under specific pathogen-free (SPF) conditions with a 12-hour light/dark cycle, 22 $\pm$ 2 °C, and *ad libitum* access to water and food. The experimental duration was 10 weeks, including induction, treatment, and sample collection. Mice were anesthetized by inhalation of isoflurane (2–3% for induction, 1.5% for maintenance, RWD Life Science, Cat# R510-22) using an anesthesia machine with a nose cone, and finally euthanized by cervical dislocation. C57BL/6 male mice aged 8 weeks were used in this study. To induce insulin resistance, mice were fed a 60% high-fructose (Fr) diet (F3510, Sigma, St. Louis, MO, USA) for 4 weeks. Subsequently, low-dose streptozotocin (STZ, Sigma, USA) was administered intraperitoneally at 30 mg/kg for 5 consecutive days to induce pancreatic beta-cell dysfunction and hyperglycemia. Mice were considered diabetic when fasting blood glucose levels exceeded 16.7 mmol/L for three consecutive days, as measured using a glucometer (Accu-Chek, Roche, Germany). Blood glucose levels and body weights were recorded weekly throughout the study to monitor metabolic status and disease progression.

To knock down YTHDF2 in the renal tissues of mice, adenoviral vectors carrying shRNA for NC and YTHDF2 (Heyuan, China) were administered via direct injection into the renal cortex under anesthesia to ensure targeted delivery to the kidney tissue. Prior to injection, mice were anesthetized with isoflurane, and the renal capsule was carefully exposed. Specifically, adenoviral vectors carrying shRNA for YTHDF2 or NC (1×10^9 PFU/mouse) were directly injected into the renal cortex under sterile conditions to ensure efficient gene delivery. Adenoviral vectors carrying shRNA for NC and YTHDF2 (sh-NC, 5′-UUCUCCGAACGUGUCACGUTT-3′; sh-YTHDF2-1, 5′-GATGGATTAAACGATGATGAT-3′; sh-YTHDF2-2, 5′-GACTTCTCACACTATGAGAAA-3′) were administered via renal cortex injection (1×10^9 PFU/mouse). The adenovirus-containing shRNA was then injected using a fine-gauge needle, followed by suturing of the incision. Post-injection, mice were monitored for

any adverse reactions and allowed to recover before further analysis. Oxamate (7 mg/kg) and Nala (750 mg/kg) were administered intraperitoneally once daily for two weeks. The sample size for each experimental group was n = 8 (mice/group). Mice were monitored throughout the treatment period for physiological and biochemical changes. Renal phenotypes were evaluated to confirm the development of DN model. Renal function was evaluated by measuring serum creatinine (Cre), blood urea nitrogen (BUN), and 24-hour urinary protein levels using standard enzymatic assays (Jiancheng Bioengineering Institute, Nanjing, China). Histological examination of kidney tissues was performed using hematoxylin and eosin (H&E) staining to assess glomerular and tubular changes.

Mice were randomly assigned into 9 groups (n = 6 per group unless otherwise specified) as follows: Sham group (vehicle-treated controls), DN group (diabetic nephropathy model only), DN + Oxamate group (DN mice treated with oxamate, 7 mg/kg/day, intraperitoneally; Sigma-Aldrich, Cat# O2751), DN + Nala group (DN mice treated with sodium L-lactate, 750 mg/kg/day, intraperitoneally; Sigma-Aldrich, Cat# L7022), DN + AAV-shYTHDF2 group (DN mice receiving renal cortical injection of AAV9-shYTHDF2), DN + AAV-shLDHA group (DN mice receiving AAV9-shLDHA), DN + AAV-shLDHB group (DN mice receiving AAV9-shLDHB), DN + AAV-shNC group (DN mice receiving AAV9-shRNA negative control), and DN + AAV-shYTHDF2 + AAV-shGDF15 group.

Histological Analysis

Kidney tissues were collected and fixed in 4% paraformaldehyde (PFA; Sigma-Aldrich, Cat# P6148) for 24 hours at 4 °C. Samples were dehydrated through a graded ethanol series, cleared in xylene, and embedded in paraffin. Sections of 4 µm thickness were prepared using a Leica RM2235 rotary microtome. Hematoxylin and eosin (H&E) staining was performed using standard protocols: sections were stained with hematoxylin solution (Sigma-Aldrich, Cat# MHS32) for 5 minutes, differentiated in 70% ethanol, and counterstained with eosin Y (Sigma-Aldrich, Cat# HT110116) for 2 minutes.

Stained slides were imaged using a Zeiss Axioscope 5 fluorescence and brightfield microscope (Zeiss, Germany) equipped with an Axiocam 208 color camera. Histological changes, including glomerular hypertrophy, tubular dilation, and interstitial inflammation, were evaluated by two blinded pathologists. Quantitative histopathological scoring was performed on five random fields per section using ImageJ software (8.0, NIH, Bethesda, MD, USA).

Detection of Serum Cre, BUN, and 24-hour Urinary Protein

At the experimental endpoint, blood was collected via cardiac puncture, allowed to clot at room temperature for 30 minutes, and centrifuged at 3,000 rpm for 15 minutes at 4 °C to obtain serum. Serum creatinine (Cre) and blood urea nitrogen (BUN) levels were measured using colorimetric assay kits (Nanjing Jiancheng Bioengineering Institute, China; Cre: Cat# C011-2-1; BUN: Cat# C013-2-1), according to the manufacturer's instructions.

For 24-hour urinary protein quantification, mice were placed in individual metabolic cages, and urine was collected into tubes containing 0.1% sodium azide to prevent degradation. Protein concentration was measured using a BCA protein assay kit (Beyotime, China, Cat# P0012). Absorbance was read at 562 nm using a Bio-Rad Model 680 microplate reader (USA).

Quantitative data were calculated based on standard curves and expressed as mg/24 hours for urinary protein and as µmol/L or mmol/L for Cre and BUN. All measurements were performed in triplicate, and the mean values were reported.

Cell Culture, Treatment, and Transfection

Human HK-2 cells were purchased from ATCC (CRL-2190) and were cultured in RPMI-1640 (11875-093, Gibco, Thermo Fisher Scientific, USA) complete medium. All cell lines were authenticated by short tandem repeat (STR) profiling and tested negative for mycoplasma contamination before use. To establish a high-glucose cell model, HK-2 cells were exposed to 25 mM glucose (Sigma, USA) for 48 hours. For YTHDF2 knockdown, HK-2 cells were infected with AAV9 particles carrying shYTHDF2 (MOI = 50). For plasmid transfection, cells were transfected with 2 µg of YTHDF2 overexpression vector or control plasmid using Lipofectamine 3000 (1:2 ratio) following the manufacturer's protocol. After 12 hours of culture, cells were co-transfected with sh-NC, sh-YTHDF2, or YTHDF2-overexpression AAV plasmids using Lipofectamine® 3000 reagent (L3000008, Invitrogen, USA). A total of 100 µL of the transfection mixture was slowly added to each well of a 6-well plate. Subsequently, HK-2 cells were treated with either oxamate (10 µM, O2751, Sigma, USA) or Nala (10 mM, L0722, Sigma, USA) for 24 hours. All cell lines were authenticated by STR profiling and tested negative for mycoplasma contamination before use. The shRNA sequences used were as follows: sh-NC, 5′-UUCUCCGAACGUGUCACGUTT-3′; sh-YTHDF2-1, 5′-GCAAGAUGAUGACCAUCAATT-3′; sh-YTHDF2-2, 5′-GCUGGAAUUUGUACCAUAUTT-3′.

Immunoblotting

Cells or tissues were lysed in RIPA buffer to extract protein, which was quantified by BCA reagent, separated by SDS-PAGE, and further transferred to PVDF membranes. Membranes were blocked with 5% milk for 1 hour before incubation with primary antibodies overnight at 4 °C. The primary antibodies used were: anti-Pan-Kla (1:1000, a18831, AB clonal), anti-H3K18la (1:1000, SAB5701137, Sigma), anti-NLRP3 (1:1000,

ab263899, abcam), anti-GSDMD-N (1:1000, ab215203), anti-caspase 1 (1:1000, ab207802), anti-LC3B (1:1000, ab192890), anti-p62 (1:1000, ab109012), anti-YTHDF2 (1:1000, ab220163), anti-GDF15 (1:1000, ab206414), and β-actin (1:3000, ab8226). After washing, membranes were incubated for 1 hour with HRP-conjugated secondary antibodies: anti-rabbit IgG (Cell Signaling Technology, Cat# 7074, 1:5000) or anti-mouse IgG (Cell Signaling Technology, Cat# 7076, 1:5000). Protein bands were visualized using an ECL chemiluminescence detection system (Bio-Rad, USA). Band intensities were quantified using ImageJ software (NIH, USA). For each protein, band density was background-subtracted and normalized to β-actin. Relative expression levels were calculated as the ratio of normalized values in the experimental group to those in the control group.

Cell Viability Assay

HK-2 cells were seeded at a density of 1000 cells per well in 96-well plates and cultured for 48 hours. Cell viability was assessed using the CCK-8 assay (C0078, Beyotime, China). Cells were incubated with CCK-8 reagent for 4 hours, and absorbance at 450 nm (OD_{450}) was measured using a microplate reader. Lactate dehydrogenase (LDH) release was quantified using a commercial kit (ab102526, Abcam, UK). Absorbance was measured at 450 nm using a microplate reader (Bio-Rad, Hercules, CA, USA). Cell viability was calculated as the ratio of the absorbance of treated cells to that of control cells and expressed as a percentage: viability (%) = (OD_{450} treated/OD_{450} control) $\times$ 100.

Real-Time PCR

Total RNA was extracted from mouse renal tissues and HK-2 cells using TRIzol reagent (Invitrogen, USA, Cat# 15596018) according to the manufacturer's instructions. RNA concentration and purity were assessed using a NanoDrop 2000 spectrophotometer (Thermo Fisher Scientific, USA). Subsequently, 1 µg of RNA was reverse-transcribed into cDNA using M-MLV reverse transcriptase (Promega, USA, Cat# M1701). Quantitative real-time PCR was performed using SYBR Green Master Mix (Takara, Japan, Cat# RR420A) on a StepOnePlus™ Real-Time PCR System (Applied Biosystems, USA). Each 20 µL reaction mixture contained 10 µL SYBR Green mix, 0.4 µL of each primer (10 µM), 2 µL of diluted cDNA, and 7.2 µL nuclease-free water. The thermal cycling conditions were: 95 °C for 30 s, followed by 40 cycles of 95 °C for 5 s and 60 °C for 30 s. Relative gene expression was calculated using the $2^{-\Delta\Delta Ct}$ method, normalized to GAPDH as the internal reference. All reactions were run in triplicate. The cDNA was amplified using the following primer sequences: mouse primers (YTHDF2: Forward 5′-GAGCAGAGACCAAAAGGTCAAG-3′; Reverse 5′-CTGTGGGCTCAAGTAAGGTTC-3′; GDF15: Forward 5′-TGTGAGGAGCTGCTGTTGTT-3′; Reverse 5′-ACAGTTCCAGGAGGTCCTTG-3′; GAPDH: Forward 5′-AATGGATTTGGACGCATTGGT-3′; Reverse 5′-TTTGCACTGGTACGTGTTGAT-3′; Human primers: YTHDF2: Forward 5′-AGCCCCACTTCCTACCAGATG-3′; Reverse 5′-TGAGAACTGTTATTTCCCCATGC-3′; GDF15: Forward 5′-GACCCTCAGAGTTGCACTCC-3′; Reverse 5′-GCCTGGTTAGCAGGTCCTC-3′; GAPDH: Forward 5′-TGTGGGCATCAATGGATTTGG-3′; Reverse 5′-ACACCATGTATTCCGGGTCAAT-3′.

ELISA

Lactylation, IL-1β and IL-18 were detected using ELISA (ab65330, ab100704, and ab215539, Abcam, UK). ELISA was performed to quantify lactate, interleukin-1β (IL-1β), and interleukin-18 (IL-18) levels in biological samples. Serum was collected from mouse blood by cardiac puncture and centrifuged at 3000 rpm for 15 minutes at 4 °C. Culture supernatants were collected from HK-2 cells after 48 hours of treatment and centrifuged to remove debris. Absorbance was measured at 450 nm using a microplate reader (Bio-Rad, Hercules, CA).

Immunostaining Assay

Renal tissues were fixed with 4% paraformaldehyde (PFA; Sigma-Aldrich, Cat# P6148), blocked with 5% BSA (Sigma-Aldrich, Cat# A9647) in PBST, and incubated with primary antibody against Pan-Kla (1:200, a18831, ABclonal). After washing, samples were incubated for 1 hour at room temperature with fluorophore-conjugated secondary antibodies: Alexa Fluor 555-conjugated goat anti-rabbit IgG (Invitrogen, USA, Cat# A-21428, 1:500) and Alexa Fluor 488-conjugated goat anti-mouse IgG (Invitrogen, USA, Cat# A-11001, 1:500). Cell nuclei were stained using DAPI (4′,6-diamidino-2-phenylindole; Sigma-Aldrich, Cat# D9542, 1 µg/mL) for 5 minutes. Images were captured using a Zeiss Axioscope 5 fluorescence microscope (Zeiss, Germany) equipped with an Axiocam 208 color camera.

CHIP Assay

Chromatin immunoprecipitation (ChIP) assays were conducted using the SimpleChIP® Enzymatic Chromatin IP Kit (Cell Signaling Technology, Cat# 9003) following the manufacturer's protocol. HK-2 cells were seeded at a density of 2 $\times$ 10^6 cells per 10 cm dish and treated as indicated. Cells were cross-linked with 1% formaldehyde (Sigma-Aldrich, Cat# F8775), and chromatin was sheared into fragments of approximately 200–500 base pairs using sonication. DNA-protein complexes associated to the target protein were immunoprecipitated using specific antibodies. After reversing the cross-links, DNA was purified. The presence of GDF15 promoter in the purified DNA was then analyzed by using qPCR using the following validated primer pairs specific to the YTHDF2 promoter region: Forward, 5′-CGGGCTAGAGGAAGTTCCTG-3′; Reverse, 5′-TCCCTGGCTTTGACCTCTTC-3′.

Human Samples

To validate the key findings, renal biopsy tissues were collected from patients diagnosed with diabetic nephropathy (n = 10) and from non-diabetic nephropathy patients undergoing renal biopsy for other kidney diseases (n = 10). These samples were obtained at The First Clinical Medical School of Anhui University of Chinese Medicine (from 2023-09 to 2024-9). The study was approved by the hospital's Ethics Committee (Approval No. 2024-N(H)-033), and informed consent was obtained from all participants. All procedures were performed in accordance with the ethical principles outlined in the Declaration of Helsinki. Patients with other systemic diseases or insufficient clinical data were excluded from the study.

YTHDF2 Overexpression

To investigate the functional role of YTHDF2 in HK-2 cells, a YTHDF2 overexpression plasmid (pcDNA3.1-YTHDF2, GenePharma, Shanghai, China) or empty vector control was transfected using Lipofectamine™ 3000 reagent (Invitrogen, USA) following the manufacturer's protocol. Briefly, 2 µg of plasmid DNA was mixed with 3 µL of Lipofectamine™ 3000 reagent in Opti-MEM (Thermo Fisher Scientific, USA) and added to HK-2 cells seeded at 5×10^5 cells/well in 6-well plates. After 6 hours of incubation, the medium was replaced with fresh RPMI-1640 supplemented with 10% FBS. Transfection efficiency was confirmed by RT-qPCR and immunoblotting 24 hours post-transfection.

m6A RNA Immunoprecipitation Assay

m6A modification of GDF15 mRNA was analyzed using the Magna MeRIP™ m6A Kit (Merck Millipore, USA, Cat# 17-10499) according to the manufacturer's instructions. Total RNA was extracted from HK-2 cells using TRIzol reagent (Invitrogen, USA). A total of 300 µg of fragmented RNA was incubated with 5 µg of anti-m6A antibody (Synaptic Systems, Cat# 202003) or IgG control overnight at 4 °C with rotation. Immunoprecipitated RNA was eluted, purified, and analyzed by RT-qPCR to quantify GDF15 enrichment. Fold enrichment was normalized to input RNA.

RNA Stability Assay With Actinomycin D

To evaluate GDF15 mRNA stability, HK-2 cells were transfected with either the YTHDF2 overexpression plasmids or control vector for 24 hours. Transcriptional activity was then inhibited by treatment with actinomycin D (Sigma, USA, Cat# A9415) at a final concentration of 5 µg/mL. Cells were harvested at 0, 2, 4, and 6 hours after actinomycin D treatment. Total RNA was extracted using TRIzol reagent, and GDF15 mRNA levels were quantified by RT-qPCR. The mRNA half-life was determined by fitting decay curves using GraphPad Prism 9 software (GraphPad Software, San Diego, CA, USA).

Statistical Analysis

All data are presented as mean ± standard deviation (SD) from at least three independent experiments. Statistical analyses were conducted using GraphPad Prism 9.0. Data normality was assessed using the Shapiro–Wilk test. For comparisons between two groups, Student's unpaired two-tailed *t*-test was used for normally distributed, while the Mann–Whitney U test was applied otherwise. For comparisons among multiple groups, one-way ANOVA followed by Tukey's post hoc test was used for normally distributed data, whereas the Kruskal–Wallis test followed by Dunn's multiple comparison test was used for non-normally distributed data. Pearson correlation analysis was performed when both variables passed the normality test; otherwise, Spearman's rank correlation was used. A p-value < 0.05 was considered statistically significant. The chi-square test was applied for categorical variables in **Supplementary Table 1**, and corresponding t-values, chi-square values, and p-values were calculated and reported.

Results

Histone Lactylation is Increased in DN Renal Tissues and High Glucose (HG)-induced Tubular Epithelial Cells

To investigate the role of histone lactylation in DN, we first examined its levels in renal tissues from DN model mice and in HG-treated tubular epithelial cells (HK2 cells). Immunostaining assay of renal sections revealed increased expression of lactylation (Pan-Kla) in DN mice compared with Sham controls (Fig. 1A, $p < 0.001$). Consistently, ELISA analysis showed significantly higher levels of lactate secretion in the serum of DN mice compared to Sham controls (Fig. 1B, $p < 0.001$). Immunoblotting further revealed a significant increase in both global protein lactylation (Pan-Kla) and histone H3 lysine 18 lactylation (H3K18la) in renal tissues from DN mice (Fig. 1C, $p < 0.01$).

We next evaluated histone lactylation in HK2 cells cultured under high glucose conditions. ELISA results indicated elevated lactate secretion in HG-treated cells compared to controls (Fig. 1D, $p < 0.01$). Similarly, immunoblotting confirmed increased levels of global lactylation and H3K18la in HG-treated HK-2 cells, in line with the *in vivo* findings (Fig. 1E, $p < 0.01$). Taken together, these results indicate that histone lactylation is upregulated in DN renal tissues and HG-induced tubular epithelial cells.

Inhibition of Histone Lactylation Attenuates High Glucose-induced Renal Tissue Damage

To investigate the role of histone lactylation in DN, we examined the effects of modulating histone lactylation on renal tissues. ELISA results confirmed that lactylation levels were elevated in the serum of DN mice, while treatment with oxamate, a lactate production inhibitor, signifi-

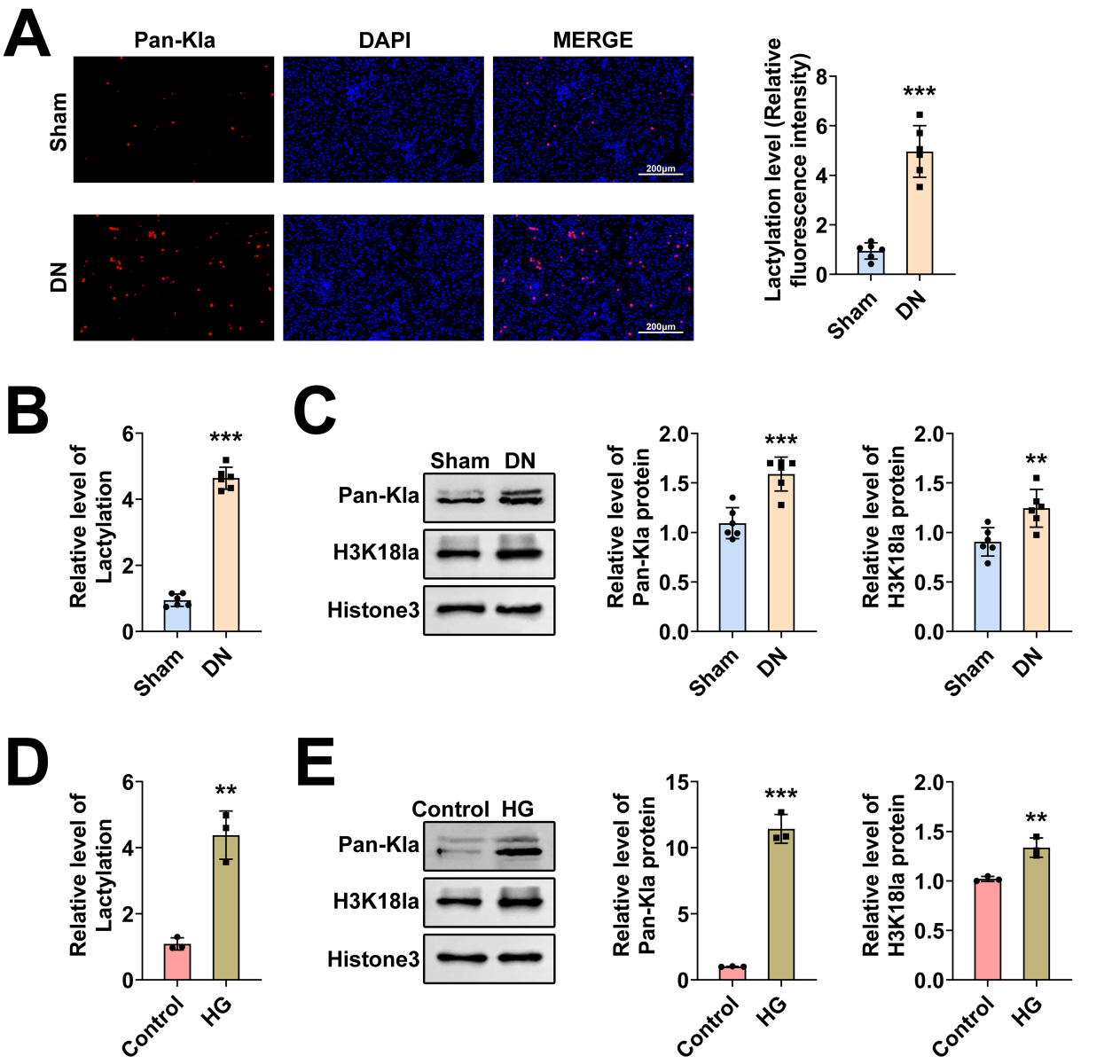

Fig. 1. Histone lactylation is increased in DN renal tissue and tubular epithelial cells. (A) Immunostaining assays detected lactylation levels (Pan-Kla) in renal tissues from DN and Sham groups. Relative Pan-Kla intensity was compared. Red panel indicates Pan-Kla. Scale bar: 200 μM (n = 6). (B) ELISA showed the secretion levels of lactylation in renal tissues from DN or Sham groups (n = 6). (C) Immunoblotting showed Pan-Kla and H3K18la expression in renal tissues from DN and Sham groups. Relative protein expression levels were compared (n = 6). (D) ELISA assays showed the secretion levels of lactylation in HK2 cells from control and HG groups (n = 3). (E) Immunoblotting showed Pan-Kla and H3K18la expression in HK2 cells from control and HG groups. Relative protein expression levels were compared (n = 3). ** $p < 0.01$, *** $p < 0.001$, HG or DN *vs* control or Sham. DN, diabetic nephropathy; HG, high glucose.

cantly reduced these levels (Fig. 2A). Conversely, administration of Nala, a lactate donor, further increased lactylation, confirming its regulatory role (Fig. 2A, $p < 0.01$). Immunoblotting yielded consistent results, with oxamate decreasing and Nala increasing both global and histone-specific lactylation (Fig. 2B, $p < 0.05$).

Hematoxylin and eosin (H&E) staining revealed pronounced renal injury in DN mice, characterized by tubular dilation, accumulation of inflammatory cells in the interstitial space, glomerular hypertrophy and sclerosis, and interstitial fibrosis. Oxamate treatment markedly mitigated these pathological features, suggesting a protective effect of lactylation inhibition (Fig. 2C). In contrast, Nala treatment aggravated renal injury, further supporting the pathogenic role of histone lactylation (Fig. 2C).

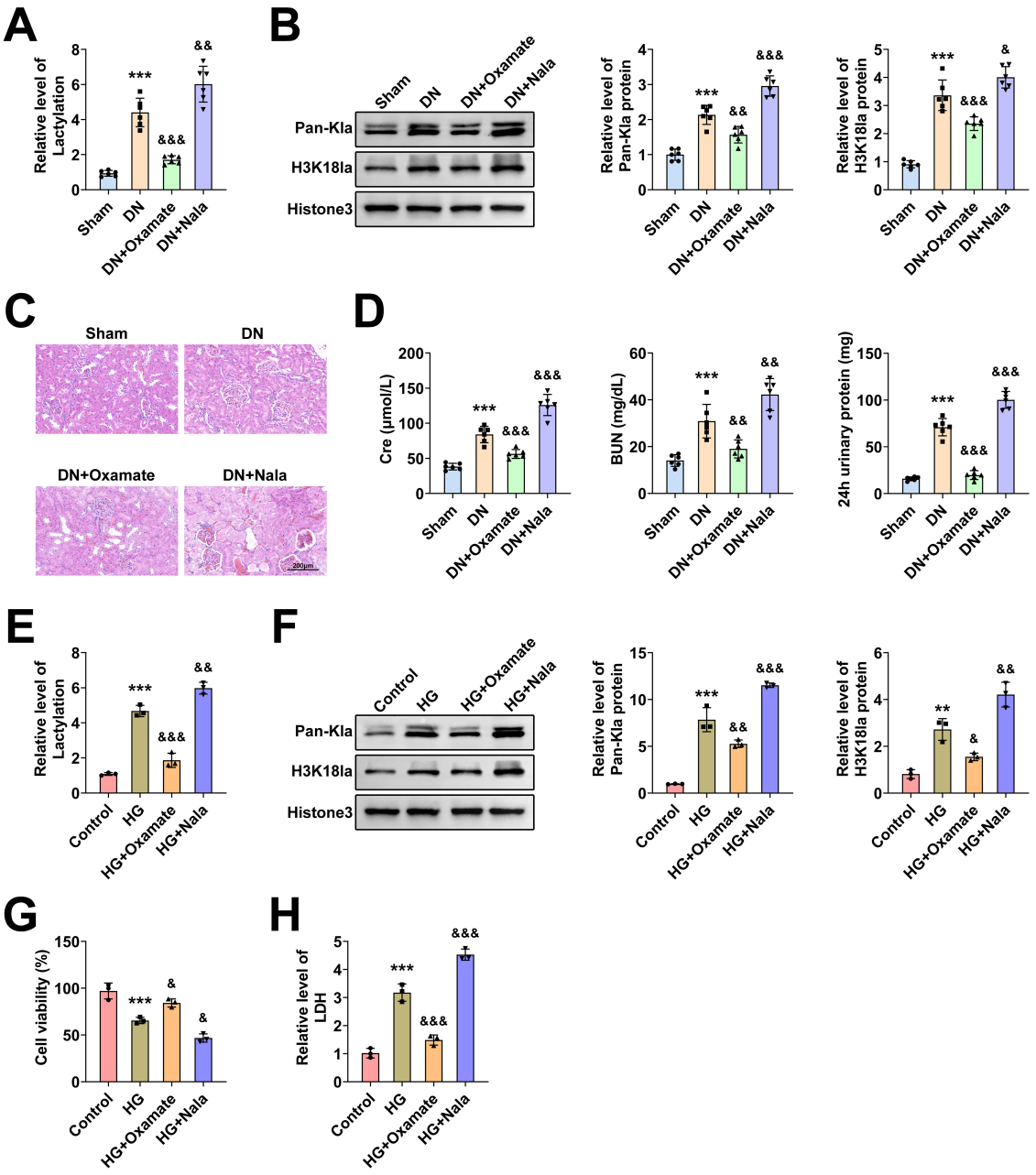

Fig. 2. Inhibition of histone lactylation alleviates renal tissue injury induced by high glucose. (A) ELISA analysis of lactylation levels in the serum from the indicated groups (n = 6). (B) Immunoblot analysis of Pan-Kla and H3K18la expression in renal tissues from Sham or DN groups treated with Oxamate (7 mg/kg) or Nala (750 mg/kg). Relative protein expression was quantified (n = 6). (C) H&E staining of renal tissues showing the degree of injury in the indicated groups (n = 6). (D) Measurements of serum Cre, BUN, and 24-hour urinary protein in Sham or DN groups following treatment with Oxamate (7 mg/kg) or Nala (750 mg/kg) (n = 6). (E) ELISA assays of lactylation levels in the supernatant of HK2 cells from the indicated groups (n = 3). (F) Immunoblot analysis of Pan-Kla and H3K18la in HK2 cells from the indicated groups, with quantification of relative expression (n = 3). (G) CCK-8 assay showing the viability of HK2 cells from the indicated groups (n = 3). (H) ELISA assays of lactylation levels in the supernatant of HK2 cells from the indicated groups (n = 3). ** $p < 0.01$, *** $p < 0.001$, HG or DN *vs* control or Sham, $^{\&}$ $p < 0.05$, $^{\&\&}$ $p < 0.01$, $^{\&\&\&}$ $p < 0.001$, Oxamate or Nala *vs* control. DN, diabetic nephropathy; H&E, hematoxylin and eosin; Cre, creatinine; BUN, blood urea nitrogen; CCK-8, cell counting kit-8; HG, high glucose.

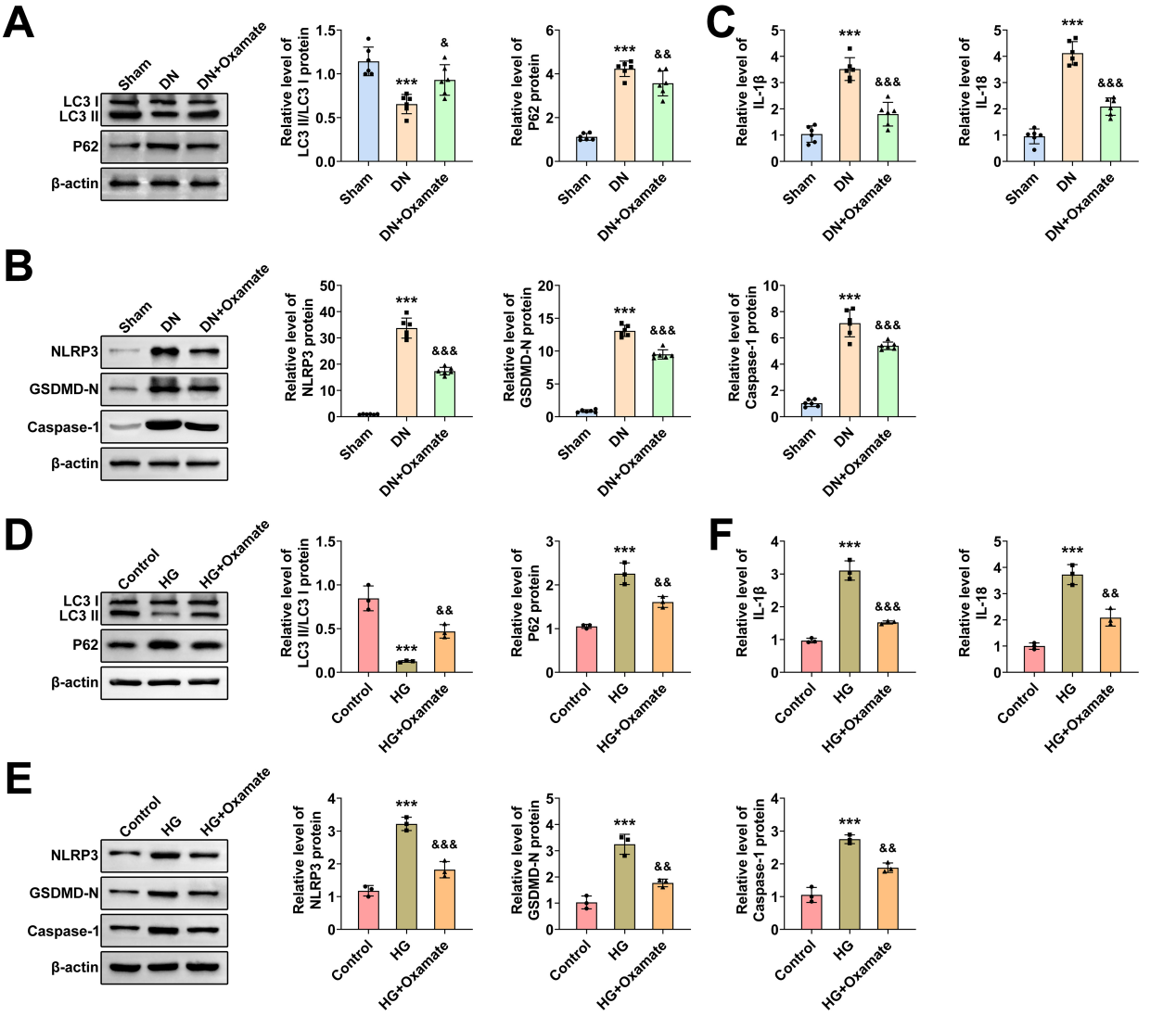

Fig. 3. Inhibition of histone lactylation promotes autophagy and suppresses pyroptosis in high glucose-induced mice and cells. (A) Immunoblot analysis of LC3 and P62 expression in renal tissues from Sham or DN groups treated with Oxamate (7 mg/kg). Relative protein expression was quantified and compared (n = 6). (B) Immunoblot analysis of NLRP3, GSDMD-N, and Caspase-1 expression in renal tissues from Sham or DN groups upon treated with Oxamate (7 mg/kg). Relative protein expression was quantified and compared (n = 6). (C) ELISA assays of serum IL-1β and IL-18 in the indicated groups (n = 6). (D) Immunoblot analysis of LC3 and P62 expression in HK2 cells from control, HG, or HG + Oxamate (10 μM) groups. Relative protein expression was compared (n = 3). (E) Immunoblot analysis of NLRP3, GSDMD-N, and Caspase-1 expression in HK2 cells from control, HG, or HG + Oxamate (10 μM) groups. (F) Relative levels of IL-1β was shown in the indicated groups. Relative protein expression was compared (n = 3). *** $p < 0.001$, HG, or DN *vs* control or Sham, $^{\&}$ $p < 0.05$, $^{\&\&}$ $p < 0.01$, $^{\&\&\&}$ $p < 0.001$, Oxamate *vs* control. DN, diabetic nephropathy; IL, interleukin; HG, high glucose.

Biochemical analyses showed that oxamate significantly reduced serum creatinine (Cre), blood urea nitrogen (BUN), and 24-hour urinary protein levels, thereby alleviating renal dysfunction. In contrast, Nala administration worsened these parameters, indicating aggravated renal injury (Fig. 2D, $p < 0.01$).

We further explored these findings using an HG-induced HK2 cell model. In line with the *in vivo* results, oxamate reduced, while Nala increased, lactylation levels in HG-treated HK2 cells (Fig. 2E, $p < 0.01$). Immunoblotting confirmed these changes by showing altered Pan-Kla and H3K18la expression (Fig. 2F, $p < 0.05$). Functional assays using Cell Counting Kit-8 (CCK-8) and lactate de-

hydrogenase (LDH) demonstrated that HG exposure suppressed cell viability and increased cytotoxicity. However, oxamate treatment reversed these effects by promoting cell growth and reducing cytotoxicity, whereas Nala further inhibited cell viability and increased cytotoxicity (Fig. 2G,H, $p < 0.05$).

To further validate the role of lactylation in DN, we knocked down LDHA and LDHB, key enzymes involved in lactate production, using AAV-shLDHA and AAV-shLDHB in both DN mice and HG-stimulated HK2 cells. ELISA results showed that lactylation levels were significantly elevated under DN and HG conditions, while LDHA/LDHB knockdown effectively reduced lactylation in renal tissues and HK2 cells (**Supplementary Fig. 1A,E**). Western blot analysis confirmed that suppression of LDHA and LDHB reduced Pan-Kla and H3K18la expression in both *in vivo* and *in vitro* models (**Supplementary Fig. 1B,F**). Functionally, LDHA/LDHB knockdown alleviated renal injury, as shown by improved renal morphology in H&E staining (**Supplementary Fig. 1C**), along with reductions in serum creatinine (Cre), BUN, and 24-hour urinary protein levels (**Supplementary Fig. 1D**). Additionally, CCK-8 assays demonstrated that LDHA/LDHB knockdown restored HK2 cell viability under HG conditions (**Supplementary Fig. 1G**), accompanied by a significant reduction in lactate secretion (**Supplementary Fig. 1H**). Collectively, these findings indicate that inhibition of histone lactylation attenuates high glucose-induced renal tissue damage and may serve as a potential therapeutic approach for DN.

Inhibition of Histone Lactylation Promotes Autophagy and Suppresses Pyroptosis in DN Cell and Mice Models

To further elucidate the protective mechanisms of histone lactylation inhibition in DN, we examined its effects on autophagy and pyroptosis in both *in vivo* and *in vitro* models. Immunoblotting indicated that DN mice and HG-induced HK2 cells exhibited a decreased LC3II/LC3I ratio and increased expression of P62, indicative impaired autophagy (Fig. 3A,D; $p < 0.001$). Treatment with oxamate rescued this phenotype, restoring autophagic activity (Fig. 3A,D; $p < 0.05$).

In parallel, immunoblotting showed elevated expression of pyroptosis-related markers, including NLRP3, GSDMD-N, and Caspase-1, in DN mice and HG-treated HK-2 cells, suggesting enhanced pyroptotic activity (Fig. 3B,E; $p < 0.001$). Oxamate treatment significantly suppressed the expression of these markers (Fig. 3B,E; $p < 0.01$). Consistent with these findings, ELISA assays demonstrated increased secretion of the pro-inflammatory cytokines interleukin (IL)-1β and IL-18 under DN and HG conditions, which was significantly reduced following oxamate treatment (Fig. 3C,F; $p < 0.01$). These results indicate that inhibition of histone lactylation promotes autophagy while suppressing pyroptosis in DN cell and mice models.

Histone Lactylation Promotes Transcriptional Activation of YTHDF2

To explore the downstream effects of histone lactylation in DN, we examined its impact on the transcriptional activation of YTHDF2. qPCR analysis revealed that renal tissues from DN mice exhibited significantly elevated YTHDF2 mRNA levels (Fig. 4A, $p < 0.001$). Treatment with oxamate suppressed YTHDF2 mRNA expression, while Nala further increased it compared to the DN group (Fig. 4A). These findings were supported by immunoblotting, which showed corresponding changes in YTHDF2 protein levels (Fig. 4B, $p < 0.001$).

Correlation analysis demonstrated a significant positive association between YTHDF2 protein expression and histone lactylation levels in renal tissues from DN mice (Fig. 4C, $p = 0.0246$).

We next validated these findings *in vitro*. In HG-stimulated HK-2 cells, YTHDF2 expression was significantly upregulated, whereas oxamate treatment attenuated its expression. This was confirmed by both qPCR and immunoblot assays (Fig. 4D,E, $p < 0.01$).

Mechanistically, as shown in Fig. 4F, H3K18la enrichment at the YTHDF2 promoter region was markedly increased in HG-treated HK2 cells compared to control cells (***$p < 0.001$), indicating lactylation-driven transcriptional activation. Notably, treatment with the lactylation inhibitor oxamate significantly reduced H3K18la binding at the YTHDF2 promoter (Fig. 4F, $p < 0.001$), further confirming the epigenetic regulation of YTHDF2 by histone lactylation.

To further confirm this association, Pearson correlation analysis was performed in DN renal tissues. A strong positive correlation was observed between Pan-Kla levels and YTHDF2 protein expression (**Supplementary Fig. 2A**; $r = 0.8602$, $p = 0.0280$), as well as between H3K18la levels and YTHDF2 protein expression (**Supplementary Fig. 2B**; $r = 0.8274$, $p = 0.0421$). Collectively, these findings indicate that histone lactylation promotes the transcriptional activation of YTHDF2, contributing to its upregulation in DN.

High Expression of YTHDF2 Aggravates Renal Injury in DN Cell and Animal Models

To evaluate the impact of YTHDF2 overexpression on renal injury, we investigated its effects in both DN cell cultures and animal models. We first observed significantly elevated expression of YTHDF2 in renal tissues from DN patients (Fig. 5A, $p < 0.001$). To assess its functional role, we employed an shRNA-expressing adeno-associated virus (AAV-shYTHDF2) to knock down YTHDF2 expression in DN mice. Immunoblotting and immunostaining confirmed effective suppression of YTHDF2 in renal tissues following AAV-shYTHDF2 treatment (Fig. 5B,C, $p < 0.001$). Notably, YTHDF2 depletion alleviated the renal injury in DN

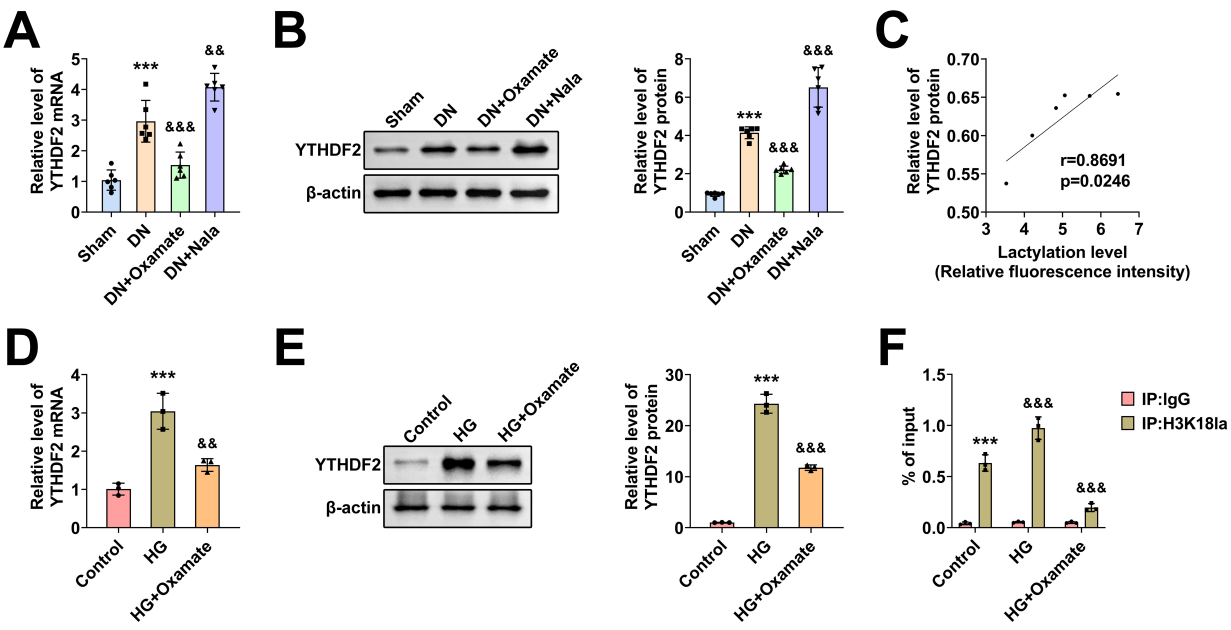

Fig. 4. Histone lactylation promotes transcriptional activation of YTHDF2. (A) qPCR analysis of YTHDF2 mRNA levels in renal tissues from Sham or DN groups upon the treatment of Oxamate (7 mg/kg) or Nala (750 mg/kg). Relative YTHDF2 mRNA expression levels are shown (n = 6). (B) Immunoblot analysis of YTHDF2 protein levels in renal tissues from Sham or DN groups upon the treatment of Oxamate (7 mg/kg) or Nala (750 mg/kg). Relative protein levels of YTHDF2 were compared (n = 6). (C) Correlation analysis of YTHDF2 protein levels and histone lactylation levels in renal tissues from DN mice. (D) qPCR assays YTHDF2 RNA levels in HK2 cells cultured under control or HG conditions with Oxamate (10 μM) or Nala (10 mM) treatment (n = 3). (E) qPCR assays indicated the mRNA levels of YTHDF2 in HK2 cells from control or HG groups upon the treatment of Oxamate (10 μM) or Nala (10 mM) (n = 3). *** $p < 0.001$, HG or DN *vs* control or Sham, $^{\&\&\&}$ $p < 0.001$, Oxamate *vs* control. (F) ChIP-qPCR analysis showing H3K18la enrichment at the YTHDF2 promoter region in HK2 cells under normal glucose (control), high glucose (HG), or oxamate treatment. H3K18la binding was significantly elevated in HG conditions and reduced following oxamate treatment. IgG served as a negative control (n = 3). *** $p < 0.001$, control + H3K18la *vs* control + IgG, $^{\&\&}$ $p < 0.01$, $^{\&\&\&}$ $p < 0.001$, HG + Oxamate + H3K18la *vs* HG + Oxamate + IgG. DN, diabetic nephropathy; ChIP, chromatin immunoprecipitation.

mice, as evidenced by significant reductions in serum Cre, BUN, and 24-hour urinary protein (Fig. 5D, $p < 0.001$).

We next assessed the effects of YTHDF2 depletion on autophagy and pyroptosis renal tissues in DN mice. Silencing YTHDF2 promoted autophagy while suppressing pyroptosis in DN mouse kidneys (Fig. 5E,F, $p < 0.01$).

Consistent with these *in vivo* findings, we performed *in vitro* experiments using HG-induced HK2 cells. Immunoblotting confirmed efficient YTHDF2 knockdown following shRNA transfection (Fig. 5G, $p < 0.01$), which was further validated by immunostaining (**Supplementary Fig. 3**). CCK-8 and LDH assays demonstrated that HG suppressed HK2 cell viability and increased cytotoxicity (Fig. 5H,I, $p < 0.01$). However, YTHDF2 depletion reversed these effects, promoting cell growth and reducing cytotoxicity (Fig. 5H,I, $p < 0.05$). Immunoblotting analysis further showed that YTHDF2 depletion promoted autophagy and suppressed pyroptosis in HG-treated HK2 cells (Fig. 5J,K, $p < 0.05$).

To validate our experimental findings in human samples, we examined renal biopsies from patients with biopsy-confirmed DN and age-matched healthy controls (n = 10 per group). As shown in **Supplementary Table 1**, DN patients exhibited significantly elevated fasting blood glucose (FBG), HbA1c, urinary albumin-to-creatinine ratio (ACR), and serum uric acid (UA) levels, along with decreased urinary creatinine (UCR) and serum albumin (ALB) levels compared to controls (**Supplementary Table 1**). These clinical parameters are consistent with impaired renal function and metabolic dysregulation in DN.

Collectively, these findings indicate that high expression of YTHDF2 aggravates renal injury in both DN cell and animal models, while its inhibition mitigates renal damage by promoting autophagy and attenuating pyroptosis, highlighting YTHDF2 as a potential therapeutic target in DN.

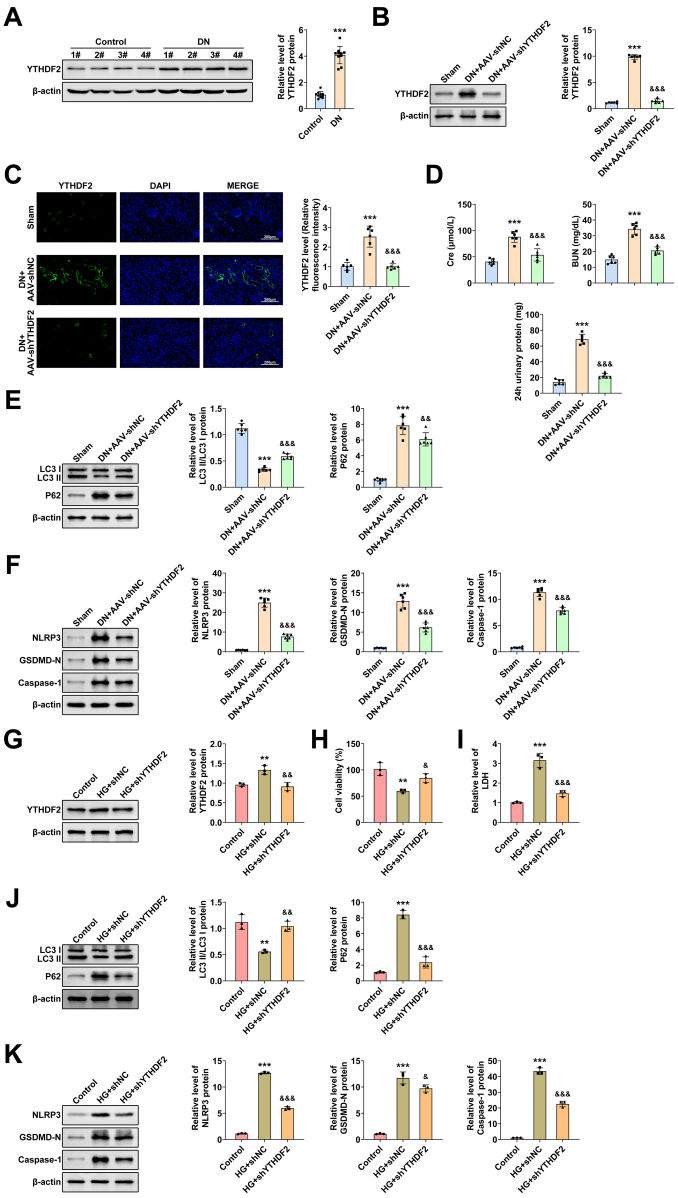

Fig. 5. High expression of YTHDF2 aggravates renal injury. (A) Immunoblot analysis of YTHDF2 in renal tissues from control and DN patients (n = 4). (B) Immunoblot analysis of YTHDF2 in renal tissues from Sham or DN groups following YTHDF2 depletion using shRNA AAV infection (n = 6). (C) Immunostaining of YTHDF2 in renal tissues from Sham or DN following YTHDF2 depletion using shRNA AAV infection (n = 6). (D) Measurement of serum Cre, BUN, and 24-hour urinary protein levels in the indicated groups (n = 6). (E) Immunoblot analysis of LC3 and P62 expression in renal tissues from Sham or DN groups following YTHDF2 depletion via shRNA adenovirus. Relative protein expression levels are shown (n = 6). (F) Immunoblot analysis of NLRP3, GSDMD-N, and Caspase-1 in renal tissues from Sham or DN groups following YTHDF2 depletion via shRNA adenovirus. Relative protein expression levels are shown (n = 6). (G) Immunoblot analysis of YTHDF2 expression in HK2 cells from the indicated groups (n = 3). (H) CCK-8 assay of HK2 cell growth in the indicated groups, measured by OD450 values (n = 3). (I) LDH levels in HK2 cells from the indicated groups (n = 3). (J) Immunoblot analysis of LC3 and P62 expression in HK2 cells from control or HG groups following YTHDF2 depletion. Relative protein expression levels are shown (n = 3). (K) Immunoblot analysis of NLRP3, GSDMD-N, and Caspase-1 expression in HK2 cells from control or HG groups following YTHDF2 depletion. Relative protein expression levels were compared (n = 3). ** $p < 0.01$, *** $p < 0.001$, HG or DN *vs* control or Sham, $^{\&}$ $p < 0.05$, $^{\&\&}$ $p < 0.01$, $^{\&\&\&}$ $p < 0.001$, sh-YTHDF2 *vs* sh-NC. DN, diabetic nephropathy; NC, negative control; Cre, creatinine; BUN, blood urea nitrogen; LDH, lactate dehydrogenase.

High Expression of YTHDF2 Promotes mRNA Degradation by Regulating m6A Modification of GDF15

We further investigated how high expression of YTHDF2 influences DN by examining its mechanistic role in regulating m6A modification of GDF15 and promoting subsequent mRNA degradation. In DN mice, GDF15 mRNA levels were significantly decreased, whereas YTHDF2 depletion restored its expression (Fig. 6A, $p < 0.001$). Similarly, immunoblot analysis indicated that knockdown of YTHDF2 led to an increase in GDF15 protein levels (Fig. 6B, $p < 0.001$).

GDF15 mRNA expression was downregulated in HG-induced HK2 cells; however, knockdown of YTHDF2 reversed this reduction (Fig. 6C, $p < 0.001$). Immunoblotting showed a corresponding change in GDF15 protein levels (Fig. 6D). The silencing and overexpression efficiency of YTHDF2 shRNA and plasmids were confirmed by qPCR and immunoblotting (Fig. 6E–H). MeRIP assays showed that YTHDF2 overexpression significantly increased m6A modification of GDF15 mRNA (Fig. 6I, $p < 0.01$). In addition, YTHDF2 was found to bind to the promotor region of GDF15 in HK2 cells (Fig. 6J, $p < 0.001$). To assess the effect of YTHDF2 on GDF15 mRNA stability, HK-2 cells were treated with actinomycin D, and YTHDF2 overexpression was shown to accelerate GDF15 mRNA degradation (Fig. 6K, $p < 0.001$). Taken together, these findings demonstrate that YTHDF2 overexpression promotes mRNA degradation by regulating the m6A modification of GDF15.

GDF15 Knockdown Reverses the Protective Effects of YTHDF2 Depletion in DN Models

To determine whether GDF15 mediates the protective effects of YTHDF2 silencing in diabetic nephropathy (DN), we performed rescue experiments by knocking down GDF15 in DN mice with YTHDF2 depletion. Immunoblot analysis confirmed that AAV-shYTHDF2 reduced YTHDF2 expression and upregulated GDF15, whereas co-infection with AAV-shGDF15 effectively diminished GDF15 levels without altering YTHDF2 expression (Fig. 7A). Histological examination revealed that YTHDF2 silencing alleviated renal injury, including tubular dilation and inflammatory infiltration, but these improvements were reversed by GDF15 knockdown (Fig. 7B). Consistently, biochemical analysis demonstrated that YTHDF2 depletion significantly reduced serum creatinine, blood urea nitrogen, and 24-hour urinary protein, while these improvements were reversed by simultaneous GDF15 knockdown, indicating worsened renal function (Fig. 7C).

We next examined autophagy and pyroptosis pathways. Western blotting showed that YTHDF2 depletion increased the LC3-II/LC3-I ratio and Beclin-1 expression while reducing P62 levels, indicating enhanced autophagy. These effects were partially abrogated by GDF15 knockdown (Fig. 7D). Moreover, pyroptosis-related proteins, including NLRP3, GSDMD-N, Caspase-1, IL-1β, and IL-18, were downregulated upon YTHDF2 silencing but re-elevated following GDF15 suppression (Fig. 7E). Taken together, these findings demonstrate that GDF15 is a critical downstream effector of YTHDF2 in regulating renal injury. The protective effects of YTHDF2 depletion are largely mediated through GDF15 restoration, highlighting the importance of the YTHDF2-GDF15 axis in DN pathogenesis.

Discussion

Diabetic nephropathy (DN) is a debilitating microvascular complication of diabetes that significantly contributes to patient morbidity and mortality, ultimately progressing to chronic renal disease and, in severe cases, end-stage renal disease [1]. The pathogenesis of DN is complex and involves metabolic, hemodynamic, and inflammatory processes, with hyperglycemia serving as the central driver of these pathways [14]. Persistent hyperglycemia triggers a cascade of deleterious cellular responses, including oxidative stress, accumulation of advanced glycation end products (AGEs), and upregulation of pro-inflammatory cytokines, all of which contribute to the progressive structural and functional damage to renal tissues [15].

A novel mechanism implicated in DN under high glucose conditions is histone lactylation, a post-translational modification of histones [16]. Recent studies have demonstrated that lactylation of the histone reader protein YTHDF2 exacerbates renal injury [17]. In this study, we focused on the role of YTHDF2 in regulating m6A modification of GDF15 and its subsequent mRNA degradation, a choice supported by bioinformatics analysis and prior studies. RNA immunoprecipitation sequencing (RIP-seq) combined with enrichment analysis identified GDF15 as a potential downstream target of YTHDF2 with significant m6A modification. Importantly, GDF15 is known for its protective role in renal inflammation, and its downregulation has been linked to aggravated kidney injury, making it a compelling target in the context of diabetic nephropathy. This process appears to be driven by increased levels of lactate, a byproduct of aberrant glycolysis often observed under hyperglycemic conditions. Lactylation of YTHDF2 enhances its ability to recognize and bind to m6A-modified transcripts, such as GDF15, which is crucial for maintaining renal integrity. GDF15 normally functions as a protective cytokine that inhibits inflammation and fibrosis pathways within the kidneys [18]. However, under hyperglycemic conditions, lactylated YTHDF2 facilitates the degradation of GDF15 mRNA via m6A mediated pathways, thereby weakening its anti-inflammatory role and contributing to the progression of renal injury in DN.

Moreover, autophagy plays a pivotal role in the pathogenesis of DN by regulating cellular homeostasis and protein turnover. In DN, autophagy serves a dual function, be-

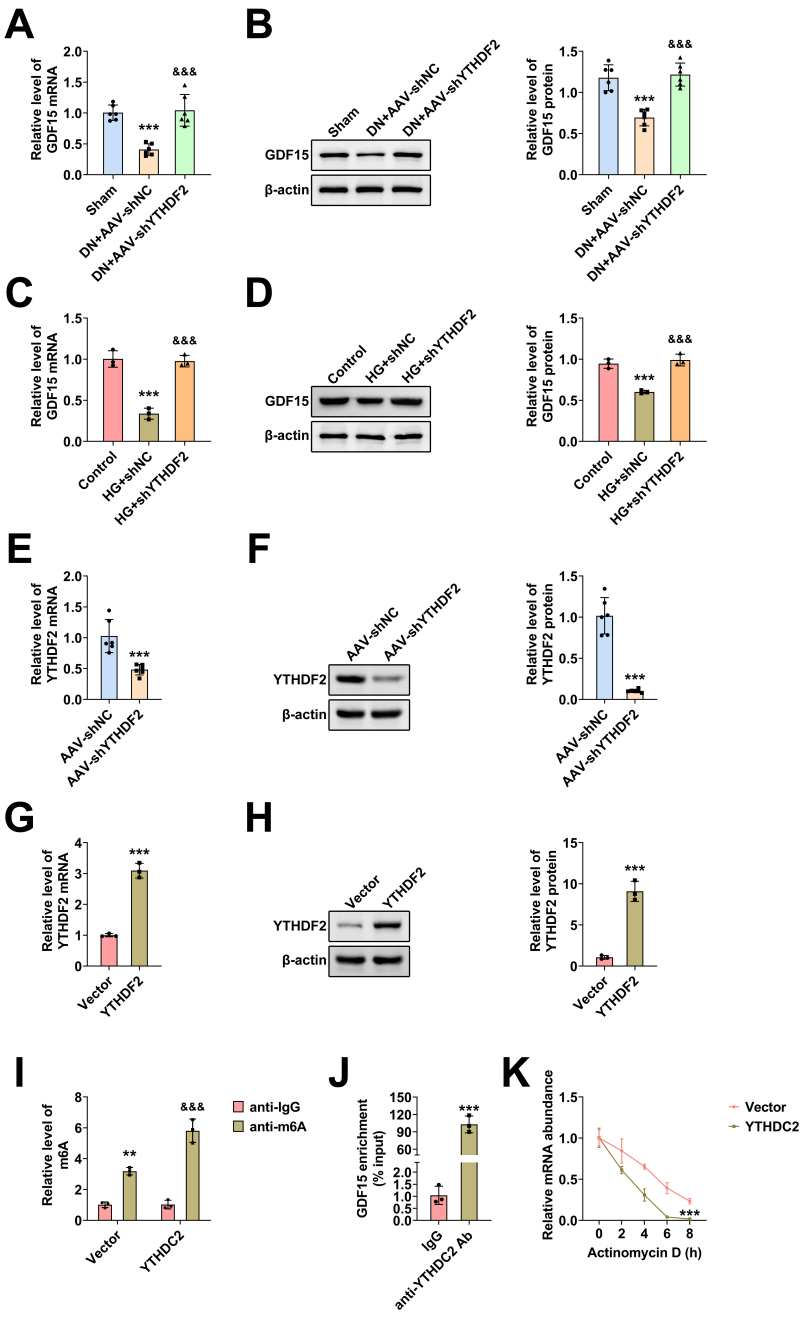

Fig. 6. YTHDF2 overexpression promotes GDF15 mRNA degradation by regulating its m6A modification. (A) qPCR analysis of GDF15 mRNA levels in renal tissues from Sham and DN groups following YTHDF2 depletion (n = 6). (B) Immunoblot analysis of GDF15 protein levels in renal tissues from Sham or DN groups following YTHDF2 depletion (n = 6). (C) qPCR analysis of GDF15 mRNA levels in HK2 cells from control and HG groups after YTHDF2 depletion (n = 3). (D) Immunoblot analysis of GDF15 protein levels in HK2 cells from control or HG groups upon the depletion of YTHDF2 (n = 3). (E) qPCR analysis of YTHDF2 mRNA levels in the indicated groups. (F) Immunoblot analysis of YTHDF2 protein levels in the indicated groups. (G) qPCR analysis of YTHDF2 mRNA levels in the indicated groups. (H) Immunoblot analysis of YTHDF2 protein levels in the indicated groups. (I) MeRIP assays showing m6A levels of GDF15 upon the YTHDF2 overexpression in HK2 cells (n = 3). (J) RIP-qPCR assays showing the interaction between YTHDC2 and GDF15 promoter (n = 3). (K) qPCR analysis of GDF15 mRNA levels in HK2 cells treated with Actinomycin D at the indicated time points (n = 3). ** $p < 0.01$, *** $p < 0.001$, HG or DN *vs* control or Sham, $^{\&\&\&}$ $p < 0.001$, sh-YTHDF2 *vs* sh-NC. DN, diabetic nephropathy; NC, negative control.

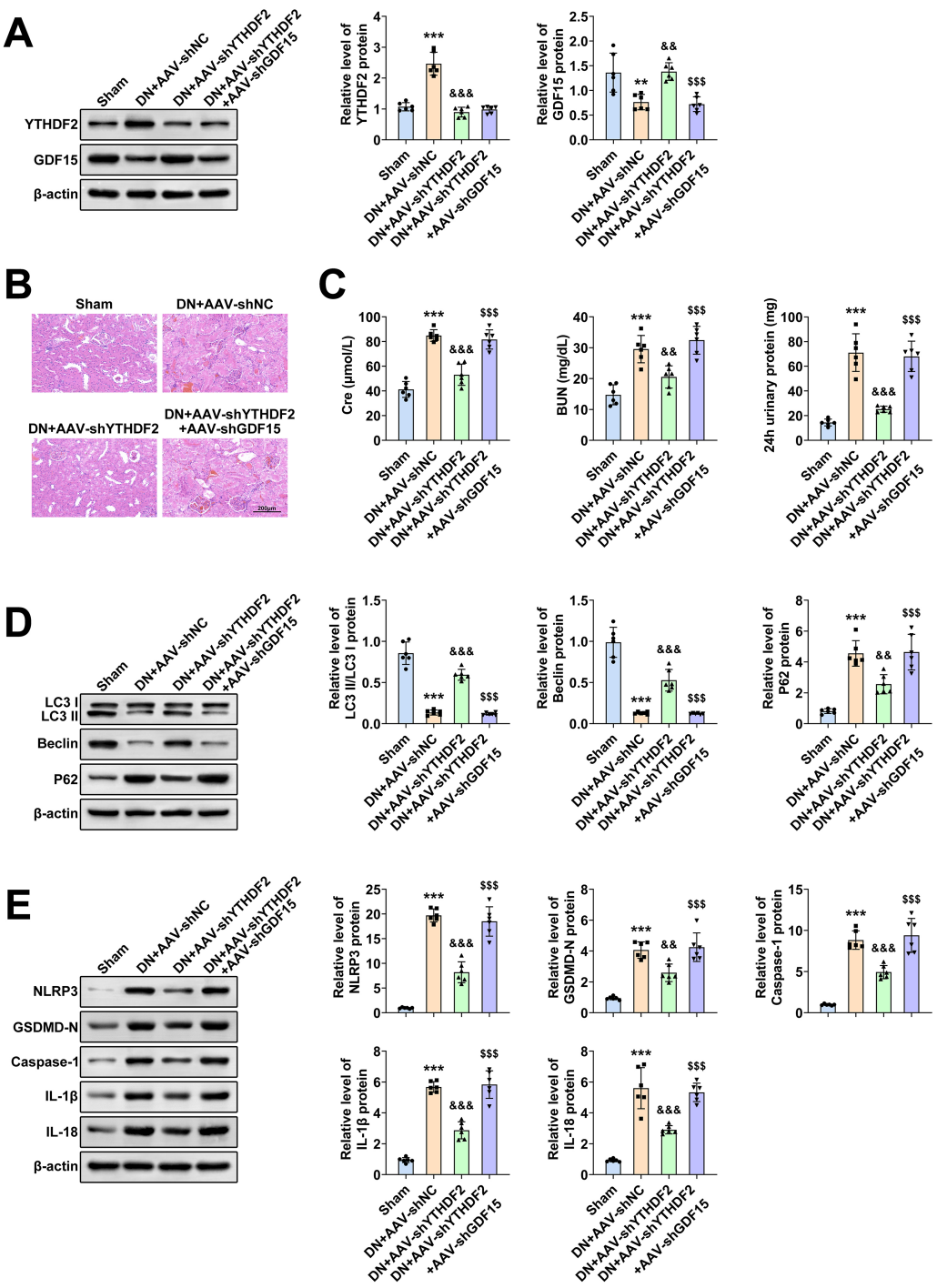

Fig. 7. GDF15 knockdown reverses the protective effects of YTHDF2 depletion in DN models. (A) Immunoblot analysis of YTHDF2 and GDF15 protein levels in renal tissues from the indicated groups: Sham, DN + AAV-shNC, DN + AAV-shYTHDF2, and DN + AAV-shYTHDF2 + AAV-shGDF15 (n = 6). (B) Representative H&E staining of kidney tissues from the indicated groups. Scale bar: 100 μm (n = 6). (C) Quantification of serum creatinine (Cre), blood urea nitrogen (BUN), and 24-hour urinary protein levels (n = 6). (D) Immunoblot analysis of autophagy markers LC3-I/II, Beclin-1, and P62 in renal tissues (n = 6). (E) Immunoblot analysis of pyroptosis-related proteins NLRP3, GSDMD-N, Caspase-1, IL-1β, and IL-18 (n = 6). ** $p < 0.01$, *** $p < 0.001$ *vs* Sham; $^{\&\&}$ $p < 0.05$, $^{\&\&\&}$ $p < 0.001$ *vs* DN + AAV-shNC; $^{\$\$\$}p < 0.001$ *vs* DN + AAV-shYTHDF2. DN, diabetic nephropathy; H&E, hematoxylin and eosin; IL, interleukin.

ing either protective or detrimental depending on the balance and timing of its activation [4,19]. Insufficient autophagy under diabetic conditions leads to the accumulation of dysfunctional organelles and proteins, thereby exacerbating cellular stress and injury. Conversely, excessive autophagy can lead to cell death and loss of renal function [20]. Histone lactylation may influence autophagic pathways by modulating the transcriptional activity of genes involved in autophagy [21]. For example, lactylation-induced activation of YTHDF2 could potentially downregulate autophagy-related genes or alter their mRNA stability, thus affecting the autophagic response to hyperglycemia [22]. In our study, YTHDF2 was selected as the primary target of investigation based on prior enrichment analysis, which identified significant histone lactylation marks on its promoter. YTHDF2 is a key regulator of m6A-modified transcripts, and its regulatory relevance has been further supported by published studies linking YTHDF2 to inflammatory and metabolic diseases.

To validate these findings, we performed ChIP-qPCR to confirm the enrichment of histone lactylation on the YTHDF2 promoter. Additionally, enrichment integrating RNA-seq and histone modification data was conducted to identify potential downstream targets regulated by histone lactylation in DN, further supporting YTHDF2 as a candidate for further investigation.

GDF15 is a distant member of the transforming growth factor-beta (TGF-β) superfamily and has gained significant attention for its protective roles in various diseases, including DN [23]. It is broadly expressed across multiple tissues, particularly under conditions of stress, injury, or inflammation. Notably, GDF15 levels are elevated in both acute and chronic inflammatory states, making it a potential biomarker and therapeutic target for DN [24]. In the context of DN pathophysiology, GDF15 plays a crucial role by modulating renal inflammation and fibrosis [25]. It functions as an anti-inflammatory cytokine by inhibiting key signaling pathways involved in the production and activity of pro-inflammatory mediators, thereby reducing tissue damage and preserving renal function. While GDF15 represents a key downstream target mediating YTHDF2's effects in DN, it is important to acknowledge that, as an m6A reader, YTHDF2 likely regulates a broader network of transcripts contributing to renal pathology.

Given the intricate interplay between hyperglycemia-induced histone modifications and autophagy, targeting these mechanisms may provide new therapeutic avenues. Modulating histone lactylation and enhancing autophagy could help restore the balance required for renal cell survival and function. Therapeutic strategies that target these pathways could potentially alleviate the progression of DN by stabilizing GDF15 levels and optimizing autophagic flux, thus offering a dual approach to address both the inflammatory and metabolic challenges of diabetic renal disease [13]. Histone lactylation has been shown to regulate the expression of genes involved in inflammatory pathways and may promote pyroptosis by activating inflammasomes such as NLRP3. This epigenetic modification enhances the transcription of pro-inflammatory mediators, thereby intensifying the inflammatory cell death observed in DN. Altogether, these findings highlight the potential of targeting epigenetic and cellular process modulation as promising strategies for managing and treating this complex condition.

RNA modification through m6A has also emerged as a crucial regulatory mechanism in various biological processes, including the progression of DN. As the most abundant internal modification in eukaryotic mRNA, m6A significantly influences RNA stability, splicing, translation, and degradation [26]. In DN, m6A modification contributes to disease pathophysiology by modulating gene expression related to inflammation, fibrosis, and cellular stress responses. Key enzymes involved in m6A regulation include methyltransferases (writers), demethylases (erasers), and m6A-binding proteins (readers), which collectively shape renal responses under diabetic conditions. The dynamic and reversible nature of m6A allows for rapid adaptation of renal cells to fluctuating glucose levels and metabolic stress, characteristic of diabetes [27]. Among these regulators, the m6A reader protein YTHDF2 has been shown to play a pivotal role in DN by recognizing and binding m6A-modified transcripts that regulate critical aspects of renal pathology.

In a high-glucose environment, increased lactylation of YTHDF2 can enhance its binding affinity for m6A-modified transcripts of GDF15. Under normal conditions, GDF15 functions as a protective cytokine that mitigates renal inflammation and fibrosis. However, hyperglycemia-induced lactylation promotes YTHDF2 activation, accelerating the m6A modification and degradation of GDF15 mRNA. This reduction in GDF15 expression compromises its protective role and contributes to the progression of renal injury. This mechanism underscores a detrimental feedback loop in which hyperglycemia-induced epigenetic and post-transcriptional modifications aggravate renal injury. Moreover, the regulation of m6A on other key transcripts involved in autophagy, apoptosis, and inflammation further contributes to the complexity of DN. By modulating the stability and translation of mRNAs encoding proteins like PPAR-α and NLRP3, m6A influences the capacity of renal cells ability to cope with metabolic and oxidative stress induced by diabetes. Given the central role of m6A in regulating these crucial pathways, targeting the m6A modification machinery represents a promising therapeutic strategy in DN. Potential interventions could involve the use of small molecules designed to inhibit or enhance the activity of specific m6A writers, erasers, or readers, thereby restoring the normal function of protective genes such as *GDF15*. This approach not only deepens our understanding of the molecular mechanisms underlying DN but also paves the way for novel interventions aimed at mitigating the progression of this chronic condition.

While our study provides compelling evidence for the involvement of the YTHDF2-GDF15 axis in DN progression, several important questions remain. First, the crosstalk between histone lactylation and other epigenetic modifications (e.g., acetylation, methylation) in renal cells warrants investigation, as these modifications may cooperatively regulate gene expression under diabetic conditions. Second, the cell type-specific effects of lactylation—particularly in podocytes versus tubular epithelial cells—requires further elucidation using single-cell approaches. Third, understanding the temporal dynamics of lactylation during DN progression (early *vs* late stages) could reveal stage-specific therapeutic windows. Notably, our lactylome data reveal lactylation changes in mitochondrial genes (e.g., *PDHA1*, *COX5B*), suggesting potential effects on renal cell metabolism that extend beyond transcriptional regulation. Future studies combining cell-type-specific lactylomics with metabolic flux analysis could disentangle these complex interactions.

Although systemic YTHDF2 inhibition may pose off-target risks, our renal cortex-specific AAV-shRNA delivery demonstrates the feasibility of localized targeting. Future work should further explore kidney-selective delivery systems (e.g., renal tubule-targeting nanoparticles) to mitigate systemic effects. The central role of lactate in energy metabolism also presents significant challenges for systemic modulation of lactylation. Our oxamate experiments (7 mg/kg, renal-focused delivery) suggest that localized approaches may be required to avoid disrupting cardiac and neuronal lactate metabolism.

We prioritized mechanistic studies on YTHDF2 for three reasons: (1) its promoter showed exceptional lactylation enrichment (–log10[P] = 12.7); (2) it has been previously linked to renal inflammation; and (3) bioinformatic analyses predicted a regulatory role in GDF15 expression. Nevertheless, parallel lactylation of metabolic genes (e.g., *PDK4*, *LDHA*) is also likely to contribute to the DN phenotype. Future directions include the development of kidney-specific LDH inhibitors, lactylation-modulating nanoparticles, and tissue-targeted epigenetic editors. While we focus on YTHDF2, other lactylation-regulated genes may also contribute to DN.

Conclusion

Our study elucidates a novel mechanism by which histone lactylation promotes the transcriptional activation of YTHDF2, which in turn exacerbates renal injury under high-glucose conditions by regulating m6A modification and degradation of GDF15 mRNA. These findings provide new mechanistic insights into the epigenetic regulation of DN and suggest potential therapeutic strategies to mitigate disease progression.

Availability of Data and Materials

The datasets used and analyzed during the present study are available from the corresponding author on reasonable request.

Author Contributions

RCY, XXW, TTC, JWX contributed to the study conception and design. Material preparation and the experiments were performed by RCY. Data collection and analysis were performed by XXW and TTC. The first draft of the manuscript was written by JWX and all authors critically revised the manuscript for important intellectual content. All authors read and approved the final manuscript. All authors have participated sufficiently in the work and agreed to be accountable for all aspects of the work.

Ethics Approval and Consent to Participate

All animal experiments were approved by the Institutional Animal Use Committee of The First Affiliated Hospital of USTC (Approval No. 2023N(A)-0177). Human samples were obtained at The First Clinical Medical School of Anhui University of Chinese Medicine (from 2023-09 to 2024-9). The study was approved by the hospital's Ethics Committee (Approval No. 2024-N(H)-033). All procedures were performed in accordance with the ethical principles outlined in the Declaration of Helsinki.

Acknowledgment

Not applicable.

Funding

This work was supported by the National Natural Science Youth Foundation of China (Grant No. 81904155) and National Natural Science Foundation of China (Grant No. 82274426).

Conflict of Interest

The authors declare no conflict of interest.

Supplementary Material

Supplementary material associated with this article can be found, in the online version, at https://doi.org/10.24976/Discov.Med.202537201.204.

References

[1] Alicic RZ, Rooney MT, Tuttle KR. Diabetic Kidney Disease: Challenges, Progress, and Possibilities. Clinical Journal of the American Society of Nephrology: CJASN. 2017; 12: 2032–2045. https://doi.org/10.2215/CJN.11491116.

[2] Umanath K, Lewis JB. Update on Diabetic Nephropathy: Core Curriculum 2018. American Journal of Kidney Diseases: the Official Journal of the National Kidney Foundation. 2018; 71: 884–895. https://doi.org/10.1053/j.ajkd.2017.10.026.

[3] Jiang N, Zhao H, Han Y, Li L, Xiong S, Zeng L, *et al*. HIF-1α ameliorates tubular injury in diabetic nephropathy via HO-1-mediated control of mitochondrial dynamics. Cell Proliferation. 2020; 53: e12909. https://doi.org/10.1111/cpr.12909.

[4] Tang C, Livingston MJ, Liu Z, Dong Z. Autophagy in kidney homeostasis and disease. Nature Reviews. Nephrology. 2020; 16: 489–508. https://doi.org/10.1038/s41581-020-0309-2.

[5] Meng F, Liang Z, Zhao K, Luo C. Drug design targeting active posttranslational modification protein isoforms. Medicinal Research Reviews. 2021; 41: 1701–1750. https://doi.org/10.1002/med.21774.

[6] Millán-Zambrano G, Burton A, Bannister AJ, Schneider R. Histone post-translational modifications - cause and consequence of genome function. Nature Reviews. Genetics. 2022; 23: 563–580. https://doi.org/10.1038/s41576-022-00468-7.

[7] Chen J, Zhang M, Liu Y, Zhao S, Wang Y, Wang M, *et al*. Histone lactylation driven by mROS-mediated glycolytic shift promotes hypoxic pulmonary hypertension. Journal of Molecular Cell Biology. 2023; 14: mjac073. https://doi.org/10.1093/jmcb/mjac073.

[8] Claycombe KJ, Brissette CA, Ghribi O. Epigenetics of inflammation, maternal infection, and nutrition. The Journal of Nutrition. 2015; 145: 1109S–1115S. https://doi.org/10.3945/jn.114.194639.

[9] Yu J, Chai P, Xie M, Ge S, Ruan J, Fan X, *et al*. Histone lactylation drives oncogenesis by facilitating m^{6}A reader protein YTHDF2 expression in ocular melanoma. Genome Biology. 2021; 22: 85. https://doi.org/10.1186/s13059-021-02308-z.

[10] Yang ZJ, Huang SY, Zhong KY, Huang WG, Huang ZH, He TT, *et al*. Betaine alleviates cognitive impairment induced by homocysteine through attenuating NLRP3-mediated microglial pyroptosis in an m^{6}A-YTHDF2-dependent manner. Redox Biology. 2024; 69: 103026. https://doi.org/10.1016/j.redox.2024.103026.

[11] Fang C, He M, Li D, Xu Q. YTHDF2 mediates LPS-induced osteoclastogenesis and inflammatory response via the NF-κB and MAPK signaling pathways. Cellular Signalling. 2021; 85: 110060. https://doi.org/10.1016/j.cellsig.2021.110060.

[12] Lee Y, Choe J, Park OH, Kim YK. Molecular Mechanisms Driving mRNA Degradation by m^{6}A Modification. Trends in Genetics: TIG. 2020; 36: 177–188. https://doi.org/10.1016/j.tig.2019.12.007.

[13] Chen J, Peng H, Chen C, Wang Y, Sang T, Cai Z, *et al*. NAG-1/GDF15 inhibits diabetic nephropathy via inhibiting AGE/RAGE-mediated inflammation signaling pathways in C57BL/6 mice and HK-2 cells. Life Sciences. 2022; 311: 121142. https://doi.org/10.1016/j.lfs.2022.121142.

[14] Cleveland KH, Schnellmann RG. Pharmacological Targeting of Mitochondria in Diabetic Kidney Disease. Pharmacological Reviews. 2023; 75: 250–262. https://doi.org/10.1124/pharmrev.122.000560.

[15] Eleftheriadis T, Pissas G, Filippidis G, Efthymiadi M, Liakopoulos V, Stefanidis I. Dapagliflozin Prevents High-Glucose-Induced Cellular Senescence in Renal Tubular Epithelial Cells. International Journal of Molecular Sciences. 2022; 23: 16107. https://doi.org/10.3390/ijms232416107.

[16] Ma XM, Geng K, Wang P, Jiang Z, Law BYK, Xu Y. MCT4-dependent lactate transport: a novel mechanism for cardiac energy metabolism injury and inflammation in type 2 diabetes mellitus. Cardiovascular Diabetology. 2024; 23: 96. https://doi.org/10.1186/s12933-024-02178-2.

[17] Liu X, Jiang L, Zeng H, Gao L, Guo S, Chen C, *et al*. Circ-0000953 deficiency exacerbates podocyte injury and autophagy disorder by targeting Mir665-3p-Atg4b in diabetic nephropathy. Autophagy. 2024; 20: 1072–1097. https://doi.org/10.1080/15548627.2023.2286128.

[18] Tang Y, Liu T, Sun S, Peng Y, Huang X, Wang S, *et al*. Role and Mechanism of Growth Differentiation Factor 15 in Chronic Kidney Disease. Journal of Inflammation Research. 2024; 17: 2861–2871. https://doi.org/10.2147/JIR.S451398.

[19] Hu Q, Jiang L, Yan Q, Zeng J, Ma X, Zhao Y. A natural products solution to diabetic nephropathy therapy. Pharmacology & Therapeutics. 2023; 241: 108314. https://doi.org/10.1016/j.pharmthera.2022.108314.

[20] Parmar UM, Jalgaonkar MP, Kulkarni YA, Oza MJ. Autophagy-nutrient sensing pathways in diabetic complications. Pharmacological Research. 2022; 184: 106408. https://doi.org/10.1016/j.phrs.2022.106408.

[21] Li W, Zhou C, Yu L, Hou Z, Liu H, Kong L, *et al*. Tumor-derived lactate promotes resistance to bevacizumab treatment by facilitating autophagy enhancer protein RUBCNL expression through histone H3 lysine 18 lactylation (H3K18la) in colorectal cancer. Autophagy. 2024; 20: 114–130. https://doi.org/10.1080/15548627.2023.2249762.

[22] Sun J, Liu G, Chen R, Zhou J, Chen T, Cheng Y, *et al*. PARP1 Is Upregulated by Hyperglycemia Via N6-methyladenosine Modification and Promotes Diabetic Retinopathy. Discovery Medicine. 2022; 34: 115–129.

[23] Lasaad S, Walter C, Rafael C, Morla L, Doucet A, Picard N, *et al*. GDF15 mediates renal cell plasticity in response to potassium depletion in mice. Acta Physiologica (Oxford, England). 2023; 239: e14046. https://doi.org/10.1111/apha.14046.

[24] Yang D, He Z, Lu J, Yuan X, Liu H, Xue Y, *et al*. Downregulation of GDF15 suppresses ferroptosis and predicts unfavorable prognosis in clear cell renal cell carcinoma. Cell Division. 2023; 18: 21. https://doi.org/10.1186/s13008-023-00103-9.

[25] Arif E, Solanki AK, Srivastava P, Rahman B, Tash BR, Holzman LB, *et al*. The motor protein Myo1c regulates transforming growth factor-β-signaling and fibrosis in podocytes. Kidney International. 2019; 96: 139–158. https://doi.org/10.1016/j.kint.2019.02.014.

[26] Qi S, Song J, Chen L, Weng H. The role of N-methyladenosine modification in acute and chronic kidney diseases. Molecular Medicine (Cambridge, Mass.). 2023; 29: 166. https://doi.org/10.1186/s10020-023-00764-w.

[27] Li M, Deng L, Xu G. METTL14 promotes glomerular endothelial cell injury and diabetic nephropathy via m6A modification of α-klotho. Molecular Medicine. 2021; 27: 106. https://doi.org/10.1186/s10020-021-00365-5.